TFW-SH15-90-001

SLOPE STABILITY IN THE TRANSIENT SNOW ZONE

By

Tien H. Wu and Carolyn J. Merry

TIMBER FISH
& WILDLIFE

March 31, 1990

SLOPE STABILITY IN THE TRANSIENT SNOW ZONE

I. Mapping the Transient Snow Zone

Final Report submitted to Timber-Fish-Wildlife
Sediment, Hydrology and Mass Wasting Committee

Supplementary Research Agreement between
Washington Dept. of Natural Resources and
Ohio State University Research Foundation

Tien H. Wu and Carolyn J. Merry
Department of Civil Engineering
The Ohio State University
470 Hitchcock Hall
2070 Neil Avenue
Columbus, OH 43210-1275

March 31, 1990

Table of Contents

List of Tables

List of Figures

List of Slides

1. AVHRR image over the State of Washington
   (394 lines by 2048 pixels)
2. AVHRR image rotated to north (394 lines by 412 pixels)
3. Image rectified to UTM coordinates
4. Snow covered area, shown in blue, superposed on AVHRR image
5. GIS file of snow covered and snow free pixels

1. INTRODUCTION

Landslides are a main source of sediments that affect water quality and fish and wildlife habitats. In the Cascade Mountains of Washington, landslides occur frequently after rapid snowmelt. Particularly serious are landslides during rain-on-snow events in the transient snow zone (Berris and Harr, 1987). For the purpose of landslide hazard zonation, the first task is co map the transient snow zone. This report describes the work accomplished during the first six months of this project for mapping the transient snow zone.

2. OBJECTIVE AND SCOPE

The objective of this study is to conduct a pilot study of mapping the transient snow zone using a combination of satellite images, snow survey data, and a snowmelt model. The work done includes identification of snowlines using satellite images, evaluation of the relation between observed snowline and measured snow depth, evaluation of snowmelt models, and preparation of a map of transient snow zones for one rain-on-snow event. A formulation of landslide hazard evaluation is also given to illustrate the relation between rain on snow and landslide hazards. The two study sites, Snoqualmie and Concrete, are shown in Fig. 1 as shaded areas. The approach used to identify rhe transient snow zone is described as follows. First, the areal extent of snow cover is determined from satellite data. Next, information from snow surveys (Brunengo, 1969) are correlated with the areal snow cover to show the distribution of snow thickness. Such a map describes the state of snow cover on a specific date. Next, for a specified rainstorm falling on a given snow cover, the amount of snowmelt is estimated with a snowmelt model. The final result is a defined region within which all of the snow melts. This region is

identified as the transient snow zone for this event, based on the simplified definition that the transient snow zone is where the snowpack forms and decays within a given time period. A more consistent definition based on probability is formulated.

3. LITERATURE REVIEW

The electromagnetic properties of snow vary as a function of snow structure and liquid water content. Water equivalent is the principal snow variable in the gamma wavelengths, whereas albedo is most important at visible and near infrared wavelengths. Emissivity is most meaningful in the thermal infrared, and the dielectric constant is most significant at microwave wavelengths (Foster et al. 1987). The spectral reflectivity of snow is dependent on snow characteristics such as grain size and shape, impurity content, near surface liquid water content, depth and surface roughness, and solar elevation (NASA 1982, see Table 1).

The areal extent of snow and the mean altitude of the snowline have been delineated from Landsat Multispectral Scanner Subsystem (MSS) data products (Meier 1975; Barnes and Bowley 1974). The Landsat MSS imagery is available for a 165 x 185 km square area in four spectral regions (two visible bands of 0.5-0.6 μm and 0.6-0.7 μm , and two near-infrared bands of 0.7-0.8 μm and 0.8-1.1 μm). Landsat Thematic Mapper (TM) data provide even better spatial (30 m vs 60 m) and radiometric resolution (8-bit vs. 6-bit or 64 vs. 256 gray levels) when compared to the MSS data. Also, there are additional wavelength bands in the middle infrared for the TM sensor that allow better discrimination between clouds and snow and to examine relative levels of melting in the snowpack.

Snow his a very high albedo and strongly reflects in the visible and

near-infrared spectral bands. Thus, the area1 extent of snow can be easily mapped at these wavelengths. In MSS band 4 (0.5-0.6 μm) , wet or refrozen snow will cause a decreased reflectance when compared to dry, powder snow. TM band 5 (1.55-1.75 μm) has proven useful in cloud/snow discrimination, as the snow appears darker than clouds in the middle infrared regions. Landsat data have been used in a number of snowmelt-runoff studies. principally to map the areal extent of snow for use in predicting snowmelt-derived streamflow (Anderson et al. 1974; Rango 1981; Thompson 1975; Rango and Itten 1976; Rango and Salomonson 1976; Shafer et al. 1981; Dey et al. 1983; Martinec and Rango 1981; Rango and Martinec 1979; Martinec 1975, 1982). A quantitative measure of the water equivalent of the snowpack has not been obtained from Landsat data. Merry and Miller (1987) provided a comprehensive literature review for remote sensing of snow cover.

Barnes and Bowley (1974) describe a set of techniques for satellite snow mapping. They also discuss problems with using satellite data to map snow cover. One problem is cloud obscuration for the visible and infrared systems. Passive and active microwave sensor systems may be a means to overcome this. Interpreting the satellite data is another problem and includes distinguishing between snow and clouds, identifying snow in densely forested areas and in areas within mountain shadows, distinguishing between snow and highly reflective rock types, and mapping irregular, patchy or discontinuous snowlines (Barnes and Bowley 1974).

Deriving snow water equivalent information from remote sensing data is still in the research phase. Promising wavelength regions include the microwave region. The microwave region provides an all-weather observing capability because microwaves will penetrate clouds and most precipitation types. Empirical relationships between passive microwave and snow water

equivalent can be derived for specific areas, such as large, flat and low-lying vegetation, and can likely be used to estimate water equivalent or snow depth.

Recently, geographic information system (GIS) techniques have been used to integrate information on snow cover derived from remote sensing with other data files. For example. Ferris and Congalton (1989) created a GIS for the Colorado River watershed to estimate snowpack water volume using elevation data and NOAA Advanced Very High Resolution Radiometer (AVHRR) satellite imagery.

4. METHODS AND RESULTS

4.1 Satellite Data

A query was made of the National Oceanic and Atmospheric Administration (NOAA) and the Earth Resources Observation System (EROS) Data Center archives to determine the availability of satellite imagery from 1975 to the present time over the Cascade Mountains. Computerized listings of NOAA, AVHRR, Landsat MSS and TM, and the French Satellite Pour l'Observation de la Terre (SPOT) High Resolution Visible (HRV) images were acquired. The list of available scenes was compared to the dates of rain-on-snow events in rhe Cascades and local weather data to determine suitable cloud-free scenes for the study.

The choice of satellite scenes was made after consultation with S. Bernath and M. Brunengo of the Washington Dept. of Natural Resources. Brunengo provided us with a list of historic storms. Suitable Landsat images were found to be available for significant rain-on-snow events in January 1976, November 1977 and January 1963. In addition, we considered the storm events that occurred between December 1988 and April 1989, which is the period

of the field study conducted by Harr et al. (1989). It was the opinion of Bernath and Brunengo that the mapping of snow cover should be done for the period of Harr's study.

The spatial resolution is 1.1 km for the AVHRR Local Area Coverage [LAC] data, 80 m for MSS. 30 m for TM, and 20 m (multispectral mode) and 10 m (panchromatic mode) for the SPOT data. For the statewide map, the 1.1 km resolution imagery is considered to be adequate to show the major features. Finer spatial resolution may include too many local details. AVHRR data are available every 12 hours daily over the state of Washington, resulting in more opportunities to obtain cloud-free imagery. As a result. three AVHRR scenes (16 December 1988. 8 February 1989 and 12 April 1989) were selected as a representative sample for the 1988-89 snow season. As the project evolves, it may be desirable to determine the transient snow zone with better accuracy in certain localities or for additional dates. This can be done with MSS, TM or SPOT data to obtain a finer spatial resolution.

The NOAA satellite is at an altitude of 833 km. The spatial resolution is 1.1 km for the LAC data and the radiometric resolution is 10-bit (1024 gray levels). The spectral band coverage for the AVHRR sensor is shown in Table 2.

The first image received and analyzed was an 8 February 1989 AVHRR scene acquired by the NOAA-11 satellite (slide 1) at nighr (1035 GMT). The original image appears rotated 180° because the data were acquired on the descending path of the NOAA satellite. The E-L! dimension is over 2000 km, and the N-S dimension is about 400 km. The Pacific Ocean appears on the right part of the slide and the Cascade Mountains appear on the left. Since the image was acquired at night, the first two channels were not usable. Therefore, the thermal bands (channel 3 and 4) were examined.

The AVHRR scene was analyzed on an ERDAS image processing system operating on a Dell PC and the VAX 8530 computer located at the Center for Mapping, The Ohio State University. The data were rotated 180' to orient the image to true north, and a subarea of 394 rows by 410 pixels was selected, which was centered over the Cascades (slide 2). Puget Sound can be seen in the upper left central part of the image. The Cascades are aligned from north-to-south along the right half of the slide. The image shown in slide 2 was recorded in channel 4. a thermal channel. The warmest temperatures are the darker tones, i.e., the water pixels. The coldest temperatures shown are the brighter tones, i.e., the snow-covered areas in the Cascade Mountains.

The digital count values (ranging from 0 to 1024) from the data tape were converted and calibrated to brightness temperatures (in degrees Kelvin) using the procedure outlined by NOAA (1988) (slide 3). The gray levels corresponding to the calculated temperature values were density-sliced and viewed on a color monitor. The lighter gray tones represent the warmer temperatures and the darker tones represent the cooler temperatures. The distribution of the gray levels was compared to ground measurements of rhe snow and to the elevation map, until the best represented snowline was delineated on the image (slide 4).

The image was rectified to the Universal Transverse Mercator (UTM) coordinate system using seven ground control points (GCPs) located on the Concrete 1:250,000 scale topographic map (slide 5). Tine corresponding pixels for these GCPs were located on the image. A cubic convolution resampling procedure was used to rectify the AVHRR image to the UT?? map coordinate system.

A GIS file was created from the classification map to define two classes: snow-free and snow-covered pixels (slide 6). The GIS file was

rectified with the seven GCPs using the nearest neighbor resampling procedure. The data file was then transferred into the Arc/Info program to overlay with the other GIS files.

A similar procedure was used to process the December and April AVHRR data sets. However, channel 2. a near-infrared channel, was used to map the snowline for these two dates, since the two images were acquired in the daytime. The near-infrared channel showed the best distinction between snow-covered and snow-free areas.

The snowline for these two dates was delineated using a level slicing technique, similar to the technique used for the February image. Successive grey levels were examined on the color monitor to display and determine the areal extent of the snowline. Snow course measurements and the elevation map were also used as ancillary data to aid in our analysis.

In the Arc/Info program an elevation array was coded in at a 1.1 km spacing for two areas in the Cascades: 48°15'-48°45'N/121°30'-122°W (Snoqualmie) and from 47°-47°30'N/121°-122°W (Concrete) (Fig. 1). In addition, the major streams were digitized as a line overlay. The snow course site locations were digitized as a point overlay.

Fig. 2 shows the snowlines derived from the AVHRR images (solid black line) superposed on the elevation maps for the Snoqualmie and Concrete sites. The AVHRR image for 12 April 89 shows clouds over the Snoqualmie sire. Therefore, the snowline in this area could not be mapped for this date.

A check on the accuracy of the snowlines can be made by comparison with the measured snow depths. The snowline delineates areas with and without snow. This is compared with snow depths measured at the stations shown in Figure 2. in Table 3 ire listed the measured snow depths and whether the

station has snow according to the AVHRR snowline. The AVHRR images correctly identified the presence of snow for snow depths greater than 8". For snow depths ranging from 1 to 7 inches, the spatial resolution of the sensor may prevent the detection of snow.

One of the advantages of using satellite data is the ability to map a region since ground surveys provide data only at isolated points. The elevation of the AVHRR snowline varies over a region, which is expected to reflect local influences such as slopes, aspect. vegetation, and topographic elevation. To study this problem further. the AVHRR snowline is compared with the mean snowline. The mean snowline (dashed black line in Fig. 2) is the elevation where the probability of finding snow, P[d>0], where d = snow depth, is 0.5. The mean snowline was calculated from Brunengo's (1989) statistics.

For the Snoqualmie site, the AVHRR image for 16 December 1988 shows little snow over the southern half of the site. This may be the result of the nonuniform spatial distribution of snow depth. A snowfall occurred on 13-14 Deccember 1988. Since 15 December 1988 was cold, snow falling from the tree canopy is not likely to be an important factor. However, strong winds in the Stampede Pass region (23-27 knots) could have blown the snow from tree tops (Brunengo, 1990). This question remains unresolved at present.

The 8 February 1989 AVHRR snowline for the Snoqualmie site is roughly parallel to, but is at a higher elevation than, the mean snowline. The difference in elevation is analyzed in Sec. 4.2. Local variations in the elevation of the AVHRR snowline are noticeable. The snowline is lower on the north-facing slope than on the south-facing slope of Grass Mountain and Cougar Mountain. It is also lower at the heads than at the lower portions of rhe east-west trending valleys.

For the Concrete sire, the AVHRR snowlines for 16 December 1988 show much

less snow than the mean. The snowlines for 8 February 1989 and 12 April 1989 are closer to the mean snowlines. Important local departures are noted, especially in the regions denoted by "a". The lack of snow in these locations is consistent in all three AVHRR images for this site (Fig. 2c,d, and e). Possible causes for these local variations include less snow because of the effect of adjacent valleys and the high ridges, Twin Sisters Mountain to the southwest, and thick vegetation (Brunego, 1990). Both the 8 February 1989 and 12 April 1989 images were acquired several days *after* a snowfall. Therefore, snow may be present, but is masked under a forest canopy. In addition, the presence of snow at Darrington (8") agrees with the AVHRR snowline that shows snow in the valley. The snow on the south side of the valley is most likely the effect of shadows from the mountains (Bruengo, 1990) that is another local condition not reflected in the mean snowline.

4.2 Snow Depth

The snow depth, d, is treated as a vector whose components are time (t), space (x-y coordinates), and elevation (e). Measured data on snow depth at a given location and time may be used to obtain the probability of snow on the ground, $P[d>0]$ and the probability distributions of depth, given there is snow, $P[d \le d_1 | d>0]$ (Thorn 1966). Brunengo (1989) has shown that the distribution for the central Cascades may be approximated by the log-normal distribution, N[u] where u=ln d. For the same region, the spatial (x,y) average of the snow depth at a given date, t and elevation. e is $\bar{d}$ Brunengo (1989) has proposed the relation,

$$\bar{u} = 3.846 + 4.148t - 1.661t^2 + 1.447e - 0.226e^2 + 0.557te \qquad [1]$$

where $\bar{u}$ = mean of ln d , t = .01 x number of days after August 31, e = .001

x elevation in feet. The value of $\bar{u}$ is the average value for about 15-40 years of weather records at 25 sites in the central Cascades. For the moment, this relation is taken to represent both the North and central Cascades as the "global spatial average." Subsequent evaluation of snow data from the North Cascade* may justify using different averages for the two regions.

For each elevation value within the GIS developed for the Cascades, Eq. [1] was used to convert the elevation into a predicted snow-depth value (Fig. 3). The AVHRR snowline and measured snow depths are also shown in Fig. 3. For comparison with the observed data, we should recognize that Eq. [1] gives the global spatial average for any given date, t while the snowline derived from the satellite image on that date represent* only one sample in time. However, the satellite image also includes the spatial component of the snowline.

We first account for the probability of the snow depth and the snowline on the date of the measurement. Fig. 4 shows the hypothetical profile (x,z) with snow depth, d. The average position of the snowline is at $(\bar{x}_o, \bar{z}_o)$ and is associated with the mean depth $\bar{d}^*$ at the station x^*, z^*. On a given day $(t=t_1)$, the snow depth is $d=d_1^*$ at x^*, z^*. On the same day, the snowline is at $x_{o,1}$, $z_{o,1}$ and this even: is associated with the measured depth d_1^* Less snow than d_1^* also means a higher elevation snowline. or

$$P[z_o \geq z_{o,1}] = P[d \leq d_1^*] \; ; \; P[z_o < z_{o\,1}] = P\,[d > d_1^*] \qquad [2a]$$

Note also that

$$P[z_o \leq z]_x = P[d>0]_x \qquad [2b]$$

This relationship allows us to treat the snowline derived from AVHRR on a given date as a data point on the curve of snow depth. More specifically, the probability $P[z_o \leq z]$ determined from the distribution in the snowline

elevation in a sample of snowlines should correspond to Brunengo's (1989) $P[d>o]$ (shown in his Fig. 4.15c), which was determined from snow depths at different stations for the same date at different years.

The above relationship is applied to the snowline and snow depths on 8 February 1989 at the Snoqualmie site (Fig. 3b). The mean snow depth versus elevation was computed with Eq. [1]; the snow depths for cumulative probabilities, $P[d \le d_1^*]$, of 0.3 and 0.7 were computed with the equation (Brunengo, 1989)

$$\frac{P[u \le u_1^*] - P[d-o]}{P[d>o]} = N[u] \qquad [3a]$$

where $u_1^* = \ln d_1^*$ and $N[.]$ = normal probability distribution. The results are shown in Fig. 5a. Also shown are the measured snow depths and the range in elevations of the AVHRR snowline. The measured snow depths occur on either side of the mean, reflecting the spatial variability due to local conditions. The lower limit *of* the AVHRR snowline is slightly higher than the mean snowline, end the upper limit of the AVHRR snowline is about 800 ft higher. The upper limit occurs mostly on the south-facing slopes of valleys and west-facing slopes (Fig. 2b). If the agreement between the measured and average snow depths is considered close enough so that the snow depths of 8 February 1969 is accepted as the mean. then by Eq. [2a], the AVHRR snowline is also the mean for 8 February 1989.

We consider next the snow depth on 8 February 1989 at the Concrete site, (Fig. 3d). The measured depths are greater than the mean snow depth, while the average elevation of the AVHRR snowline is approximately 300 ft above the mean snowline, while the upper limit is much higher. We are unable to make more detailed comparisons because of inadequate data on measured snow depths. In addition, Brunengo's (1989) statistics may not be applicable to

the North Cascades.

To estimate the snow depths over the region for a given date we use the snowline for 8 February 1989 at the Snoqualmie site (Fig. 3b) as a" example. Consider first the regions where the AVHRR snowline is close to the mea" snowline. As a" example, these sections are indicated as 1-1 in Fig. 6. Here, it is assumed that Brunengo's mean snow depth is valid. The snow depths for areas where the AVHRR snowline departs appreciably from the mea" snowline is assumed to vary linearly with elevation, as illustrated by the dot-dashed line in Fig. 5a. The mea" snow depth (60 in. at elev. 3750 ft.) is considered correct. Examples of the extrapolated snowlines are show" at sections 2-2 in Fig. 6. Because this is only a" example to illustrate applications, the interpolation between these sections was sketched in by hand. A" interpolation scheme can be programmed, if it is decided to produce maps of snow depths.

The above example is unusual in that the measured snow depths on 8 February 1989 happen to be close to the mea" depth. For a more general case, the measured snow depths agree with the computed depth for probability $P[d<d^*] = p$. The" it is necessary to estimate the snowlines that correspond with the mean depth, $\bar{d}$ Fig. 5b shows the two conditions, where $e_{o\,u}$ and e_o equal to the upper limit of the AVHRR snowline and the snowline from Brunengo's (1989) data, respectively. The overbar and [p] denote the mea" and probability, respectively. From the limited data in Fig. 5a, we make the conservative assumption that $e_o[p]$ and $\bar{e}_o$ are also the lower limits of the AVHRR snowlines. The problem is to estimate $\bar{e}_{o,u}$ with $e_{o,u}[p]$, taken from the AVHRR snowline, and $e_o[p]$ and $\bar{e}_o$, taken from Brunengo (1989). One possible solution is to assume that:

$$e_{o\,u}[p] \; e_o[p] = \bar{e}_{o,u} \; \bar{e}_o \qquad [3b]$$

This assumption can be modified, if necessary, after checking with other sets of snow depth and AVHRR data. This approach combines the snowline from AVHRR on a given date with Brunengo's statistics to estimate the snowline for the condition of mean snow depth. Once this snowline is established, the mean snow depth as a function of e, x, y can be calculated as described in the preceding paragraph.

The above estimate of depth is limited to open areas, for which Eq. [1] is designed. The snow depth in forests may be expected to be different. Estimates of snow depths in forests may be made with the statistics in Brunengo (1989).

ii.3 Snowmelt Prediction

Several snowmelt models were reviewed in detail. These include the Corps of Engineers (1956), HYDRO-17 (Anderson, 1973), HYDRO-19 (Anderson, 1976) and the U.S. Geological Survey model (Leavesley, 1989). The Corps of Engineers' model uses precipitation, temperature, and wind velocity for estimating snowmelt. Berris and Harr (1987) found that their measured snowmelt agreed well with estimates from the Corps of Engineers model. The algorithm of the temperature index method requires only the temperature, precipitation, ad wind speed for estimating snowmelt during rainfall events:

$$M = (0.029 + 0.0084kV + 0.007R)(T-32) + 0.09 \qquad [4a]$$

where M = snowmelt, V = wind velocity, R = rainfall, T = temperature (English units), k = basin constant = 1.0 for open areas and 0.2 for densely forested areas. in alternate equation for heavily forested areas is

$$M = (0.074 + 0.007R)(T-32) + 0.05 \qquad [4b]$$

This is equivalent to taking V = 5 mph. The Corps of Engineers model was chosen because of the limitations in available weather records. All the other models require vapor pressure. in addition to wind speed and temperature, and cannot be used with the limited weather data that are available for our study area.

For the present study, we illustrate the procedure by using the storm of January 2-4, 1989 to compute the melt. This is also the storm for which Harr et al. (1989) measured the snowmelt at Finney Creek. The computed and measured snowmelts for the open area are shown in Fig. 7 as a function of time. The cumulative rain plus snowmelt for the three days are listed in Table 4. The difference between the snowmelts in forested area computed by Eq. [4a] and [4b] is due to the different wind velocity in the two equations. The accuracy of the Corps of Engineers' model is considered to be acceptable for this preliminary study.

The melt of January 2-4, 1989 was applied to the snow depth in Fig. 6. The computed snowmelt of 1.3 inches in snow water equivalent was converted to a snow depth of 4 inches. The conversion of 1 to 3 is based on the average ratio of snow water equivalent to snow depth given in Brunengo (1989). This was superposed on the snow depth map, Fig. 6, to identify the zone where snow depths up to 4 inches on February 8 would be melted. This zone is shown as shaded in Fig. 6.

4.4 The Transient Snow Zone

There exists no generally accepted and precise definition of the transient snow zone. If we adopt the simplified notion that the transient snow zone is the region where the snowpack forms and decays within a given winter, then the shaded area in Fig. 8 is the transient snow zone (given the

storm of January Z-3-4 falls on the snowpack of February 8, 1989).

As pointed out by Brunengo (1989). the definition of transient snow zone should be based on probabilities. One possibility is to define the transient snow zone in terms of the snowmelt, M, plus rainfall, R, during a rain-on-snow event, or the probability that R+M exceeds a certain value, a: P[M+R)>a]. The snowmelt, as given by Eq. [4], is a function of R,D,T,V, and d, where D = duration of rainstorm. The expression is generalized as:

$$M = g(R,D,T,V,d) \qquad [5a]$$

then

$$R+M = g(R,D,T,V,d) + P = g^{*}(R,D,T,V,d) \qquad [5b]$$

The mean and variance of R,D,T, and V have been summarized by Brunengo (1989) and the mean and variance of d are obtained as described in section 4.3.

One simple approach is the first-order second-moment method (Ang and Tang, 1975)

$$E[M] \simeq g[\bar{R}, \bar{D}, \bar{T}, \bar{V}, \bar{d}] \qquad [6a]$$

$$\text{Var}[M] \simeq \left(\frac{\partial g}{\partial R}\right)^2 \text{Var}(R) + \left(\frac{\partial g}{\partial D}\right)^2 \text{Var}(D) + \left(\frac{\partial g}{\partial T}\right)^2 \text{Var}(T) + \ldots \qquad [6b]$$

Since the distributions R,D,T,V and d are approximately log-normal, and Eq. [4] is linear, M can be represented by a log-normal distribution. Then, rhe probability of R+M exceeding a value a. P[(R+M)>a] can be found (Fig. 9). Conversely, for a given probability P, a can be found for all elevations and dates in a region. If annual weather data (mean and variance) are used to calculate the distribution of R+M, then P[(R+M)>a] is the annual probability of R+M exceeding a. If the annual probability of (R+M)>a is P_1, the return period is:

$$T_r = \frac{1}{P_1} \qquad [7]$$

Return periods can be calculated for various values of a and used to produce

maps of frequency for given values of R+M. These maps may be compared with the probabilities of precipitation. Where there is a significant difference between P of precipitation and P of R+M, then rain-on-snow events are likely to be serious. What constitutes a significant difference will be based on the intended use of the map. For mapping of landslide hazard, the significance will be determined from the sensitivity of landslide hazard to R+M.

4.5 Relationship of Transient Snow Zone to Infiltration and Landslide Hazard

To assess the risk of slope failure in the transient snow zone, we need to estimate the probable changes in the piezometric level during a rain-on-snow event. The probability that the piezometric height, h, will exceed h_1 may be written as:

$$P[h>h_1] = \int \ldots \int f(h|i)\, f(i|R,T,\ldots)\, f(R)\, f(T)\, \ldots\, dh\, di\, dR\, dT \quad . \qquad [7]$$

where h = piezometric height, i = infiltration, R = rainfall, T = temperature, and f(.) = probability density function, and P(.) = probability. In this conceptual model, we have shown only P and T as input. Other factors may be included if needed, In addition, it is assumed that P, T are statistically independent. The relation in Eq. [7] can be broken down into components as follows:

$$P[i>i_1] = \int \ldots \int f(i|R,T\ldots)\ f(R)\ \ f(T)\ \ di\ \ dR\ \ dT \qquad [8]$$

If we assume that all precipitation and snowmelt, M, are available for infiltration into the soil, then:

$$i = R + M \qquad [9]$$

For the Corps of Engineers' model. the input data are R, T, D, V, and d. This model will be used to estimate M. Snow depth at a given time of the year may be estimated by the statistical relation developed by Brunengo (1989). Temperature and precipitation data will be taken from weather data. The sensitivity of snowmelt to the inputs and correlation between input variables will be investigated and the less important components can be deleted. Eq. [6] in Sec. 4.4 may be used to estimate the mean and variance of snowmelt from the means and variances of the input variables.

An infiltration model is used to estimate $h|i$ in Eq. [7]. Available infiltration models include those of Green and Ampt (1911), Reddi (1988) and finite difference solutions (e.g. Freeze. 1971). Infiltration models require soil permeability, K, and initial soil moisture, θ_o , which are presumed to be known. Reddi's infiltration model has been programmed to compute the mean and variance from the means and variances of K and θ_o , for a given i. Estimated piezometric heights can be calibrated against measured piezometric levels, such as those being measured by Sullivan and Dietrich, and Cundy.

Instead of the integrations in Eqs. [7] and [8], a possibility is to obtain simplified solutions. A sensitivity analysis will be made to evaluate the effect of various inputs and correlations between input variables on h. As an example, consider the input of rainfall intensity, which is a random function of time and rainfall R, and duration D, and may not be independent. One possibility is to evaluate the sensitivity of h to D. It is expected that this would be a function of the retardation time, t_r:

$$t_r = \frac{h_w}{K} \qquad [10]$$

where h_w = distance from surface to water table and K = coefficient of permeability. The parameter t_r may be taken as a site characteristic that

will allow one to choose the D that produces the maximum response. An alternative approach is to assume that P and D are statistically independent (Brunengo, 1989). In this case. one can use the means of precipitation and duration as input into the snowmelt-infiltration model.

5. SUMMARY AND CONCLUSIONS

The results of this preliminary study show that AVHRR data may be used to identify snowlines. The elevation variation along the AVHRR snowlines show the spatial component of snow cover, which is a reflection of local conditions. At the Snoqualmie site, we identified the south-facing slopes as locations where the snowline is higher than the mean snowline. The AVHRR snowlines provide a measure of the spatial component that can be used to modify the average snowline as estimated from Brunengo's relation. A methodology was developed to map the mean and variance of snow depth on a given day by combining AVHRR data and snow depth measured for that day with Brunengo's statistical data predicting the average snowline and snow depth. This was done for February 1989 at the Snoqualmie site as an illustration. Interpretation of some AVHRR snowlines is handicapped by a lack of measured snow depth, unknown effects of vegetation and local topography.

The Corps of Engineers model requires input data that are available from weather records. It was found to give reasonable results when compared with snowmelt measured by Harr et al. (1989). Therefore, it provides a practical means for estimating snowmelt. It was shown that this model could be combined with the snow depth map to obtain a probability map of rain plus snowmelt. This probability map is a measure of the severity of rain-on-snow events and it is recommended that the transient snow zone be defined in terms of this probability. It was also shown that this probability map could be used to

estimate probable infiltration and landslide hazard.

6. PROPOSED RESEARCH

The results and methodologies developed in the first phase of this research make it possible to proceed to the next phase. We propose to (1) analyze another scene for the Snoqualmie site and (2) map a larger area around the Concrete site. The product of these two scenes will be used to verify the local trends observed in the 8 February 1989 maps and to identify factors that are responsible for differences between the snowline as mapped from AVHRR data and the average snowline estimated with Brunengo's statistics. The factors affecting the AVHRR-derived snowline may include the effect of vegetation cover masking the snowpack and timing of the AVHRR image relative to the storm event. Physical factors, such as local topography, may exert important influences on the spatial distribution of snow thickness. We will attempt to verify the differences noted in Fig. 2 by seeking local information on snow depth. Recommendations on what band combination is best to delineate the snowline will also be made. We anticipate that the visible/infrared AVHRR bands will be the best, with the thermal bands useful to differentiate snow from clouds.

This work will take advantage of snow data being recorded at Weather Service Stations that previously had not recorded snow depth (Brunengo, 1090). The elevation data file for the Concrete and Wenatchee 1:250,000 scale areas has been received and a Landsat-derived vegetation map in digital form exists for the region. Both will be used as input to our study.

7. REFERENCES

Anderson, D. M.. H. L. McKim, L. W. Gatto, R. K. Haugen, W. K. Crowder, C. W. Slaughter and T. L. Marlar (1974). Arctic and subarctic environmental analyses utilizing ERTS-1 imagery. Type III Final Report to NASA for the period June 1972-February 1974, Contract no. S-70253-AG, 112 pp.

Anderson, E. A. (1976). A point energy and mass balance model of a snow cover. Technical Report NWS19, U.S. Dept. of Commerce, National Oceanic and Atmospheric Administration: Washington, DC.

Anderson, E. A. (1973). National Weather Service river forecast system-snow accumulation and ablation model. Technical Memorandum NWS HYDRO-17. U.S. Dept. of Commerce, National Oceanic and Atmospheric Administration: Washington D.C.

Ang, A. H-S., and W. H. Tang (1975). Probability Concepts in Engineering Planning and Design, John Wiley & Sons Publishing: New York, 409 p.

Barnes, J. C. and C. J. Bowley (1974). Handbook of techniques for satellite snow mapping. Concord, MA: Environmental Research and Technology, Inc., Document No. 0407-F, 95 pp.

Berris, S. N. and R. D. Harr (1987). Comparative snow accumulation and melt during rainfall in forests and clear-cut plots in the western Cascades of Oregon, Water Resources Research, 23(1): 135-141.

Brunengo, M. J. (1989). Draft of Ph.D. dissertation. Univ. of Washington.

Brunengo, M. J. (1990). Comments on Draft Final Report.

Corps of Engineers (1956). Snow Hydrology. North Pacific Division, U.S. Army Corps of Engineers, Portland, OR, 437 p.

Dey, B., D. C. Goswami and A. Rango (1983). Utilization of satellite snow-cover observations for seasonal streamflow estimates in the Western Himalayas. Nordic Hydrology, pp. 257-266.

Ferris, J. S. and R. G. Congalton (1969). Satellite and geographic information system estimates of Colorado River Basin snowpack, Photogrammetric Engineering and Remote Sensing, 'Jo. 55, No. 11, pp. 1629-1635.

Foster, J. L.. D. K. Hall and A. T. C. Chang (1987). Remote sensing of snow EOS, Transactions of the American Geophysical Union, p. 681-664.

freeze, R. A. (1971). Three dimensional. transient, saturated-unsaturated flow in a groundwater basin, Water Resources Research, 7(2): 347-366.

Green. W. A., and G. A. Ampt (1911). Studies on soil physics, I. The flow of air and water through soils, Journal of Agricultural Science, 4:1-24.

Harr, R. D.. B. A. Coffin, and T. W. Cundy (1989). Effects of timber harvest on rain-on-snow runoff In the transient snow zone of the Washington Cascades, Interim Final Report to TFW Scientific, Hydrology. and Mass Wasting Committee.

Leavesley, G. (1989). Personal communication.
Martinec, J. (1975). Snowmelt-runoff model for stream flow forecasts. Nordic Hydrology, 6:145-154.

Hartinec, J. (1982). Runoff modeling from snow-covered area. IEEE Transactions on Geoscience and Remote Sensing, GE-20(3): 259-262.

Martinec, J. and A. Rango (1981). Area1 distribution of snow water equivalent evaluated by snow cover monitoring. Water Resources Research, 17(5): 1480-1488.

Meier, M. F. (1975). Application of remote-sensing technqiues to the study of seasonal snow cover. Journal of Glaciology, 15(73):251-265.

Merry, C. J. and M. S. Miller (1987). Use of Landsat digital data for snow cover mapping in the Upper Saint Johns River Basin, Maine. CRREL Special Report 87-8, U.S. Army Cold Regions Research and Engineering Laboratory: Hanover, NH, 74 p.

NASA (1982). Plan of research for snowpack properties remote sensing $(PRS)^2$, NASA Goddard Space Flight Center: Greenbelt, Maryland.

NOAA (1988). NOAA polar orbiter data users guide, NOAA National Climatic Data Center, Satellite Data Services Division: Washington, DC.

Rango, A. (1981). Application systems verification and transfer project. Vol. I. Operational applications of satellite snow cover observations--executive summary. NASA Technical Paper 1822, 81 pp.

Rango, A. and K. I. Itten (1976). Satellite potentials in snow cover monitoring and runoff prediction. Nordic Hydrology, 7:209-230.

Rango, A. and J. Martinec (1579). Application of a snowmelt-runoff model using Landsat data. Nordic Hydrology, 10(4):225-238.

Rango, A. and V. V. Salomonson (1976). Satellite snow observations and seasonal streamflow forecasts, Final Report under NOAA Contract No. NA-776-74, 19 pp.

Reddi, L. N. (1988). Probabilistic analysis of groundwater levels in hillside slopes, Ph.D. dissertation, Ohio State Univ., Columbus, OH.

Shafer, E. A., c. F. Leaf, J. A. Danielson and G. F. Moravec (1961). Operational applications of satellite snow-cover observations--Colorado Field Test Center. Applications Systems Verification and Transfer Project, Vo. IV, NASA Technical Paper 1825, 101 pp.

Thom, H.C.S. (1966) Distribution of maximum annual water equivalent of snow on the ground: Monthly Weather Review, 94(4):265-271.

Thompson, A. G. (1975). Utilization of Landsat monitoring capabilities for snowcover depletion analysis. Operational Applications of Satellite Snowcover Observations, Workshop held at South Lake Tahoe. CA, 18-21 August. NASA SP-391, pp. 113-127.

TABLE 1 Parameters Affecting Albedo and Emissivity of Snow
(after Warren 1982 and NASA 1982)

snow property	Visible Solar Albedo	Thermal Infrared Emissivity	Microwave Emissiviry
Grain (or crystal) size	Yes*	Yes	Yes
Zenith (or nadir) angle	Yes*	Yes	Yes
Snow depth	Yes†		Yes
Contaminants	Yes		
Liquid water content	Yes	Yes	Yes
Surface roughness	Yes		Yes
Density			Yes
Temperature		Yes	Yes
Stratification			Yes
Soil state, moisture roughness, vegetation			Yes

*if snowpack is thin or impurities are present
†shallow, up to a few centimeters

TABLE 2 Spectral Band Coverage for the AVHRR Sensor

EVEN-NUMBERED SATELLITES			ODD-NUMBERED SATELLITES		
Channel	Spectral Band m		Channel	Spectral Band (μm)	
1	0.58-0.68	(visible)	1	0.58-0.68	(visible)
2	0.72-1.10	(near IR)	2	0.72-1.10	(near IR)
3	3.55-3.93	(thermal)	3	3.55-3.93	(Thermal)
4	10.5-11.5	(thermal)	4	10.3-11.3	(thermal)
5	Channel 4 repeat		5	11.5-12.5	(thermal)

TABLE 3 Comparison of AVHRR Snowline with Measured Snow Depth

Location	Date	Measured Snow Depth (in)	Snow observed on AVHRR Image
Stampede Pass	16 Dec 88	32	Yes
Palmer	8 Feb 89	0	NO
Mud Mtn. Dam	8 Feb 89	0	NO
Cedar L.	8 Feb 89	2	NO
Grass Mtn. 3	8 Feb 89	7	Yes
Lester Ck.	8 Feb 89	58	Yes
Cougar ntn.	8 Feb 89	48*	Yes
Lynn L.	8 Feb 89	63	Yes
Twin Camp	8 Feb 89	63	Yes
Sawmill R.	8 Feb 89	70	Yes
Corral Pass	8 Feb 89	59	Yes
Concrete	16 Dec 88	0	NO
Concrete	8 Feb 89	1	NO
SF Thunder Ck.	8 Feb 89	8	No
Darington	8 Feb 89	8	Yes
Schreibers Mdw.	8 Feb 89	92	Yes
Watson L.	8 Feb 89	104	Yes

TABLE 4 Computed and Measured Rain plus Snowmelts

Date	Rain plus Snowmelt in Clearcut (mm)		Rein plus Snowmelt in Forest (mm)		
	Meas.	Comp.	Meas.	Comp. Eq. [4a]	Comp. Eq. [4b]
Jan 2	14	20	16	21	20
Jan 3	83	56	45	50	42
Jan 4	5	4	4	5	3
Total	102	80	65	76	65

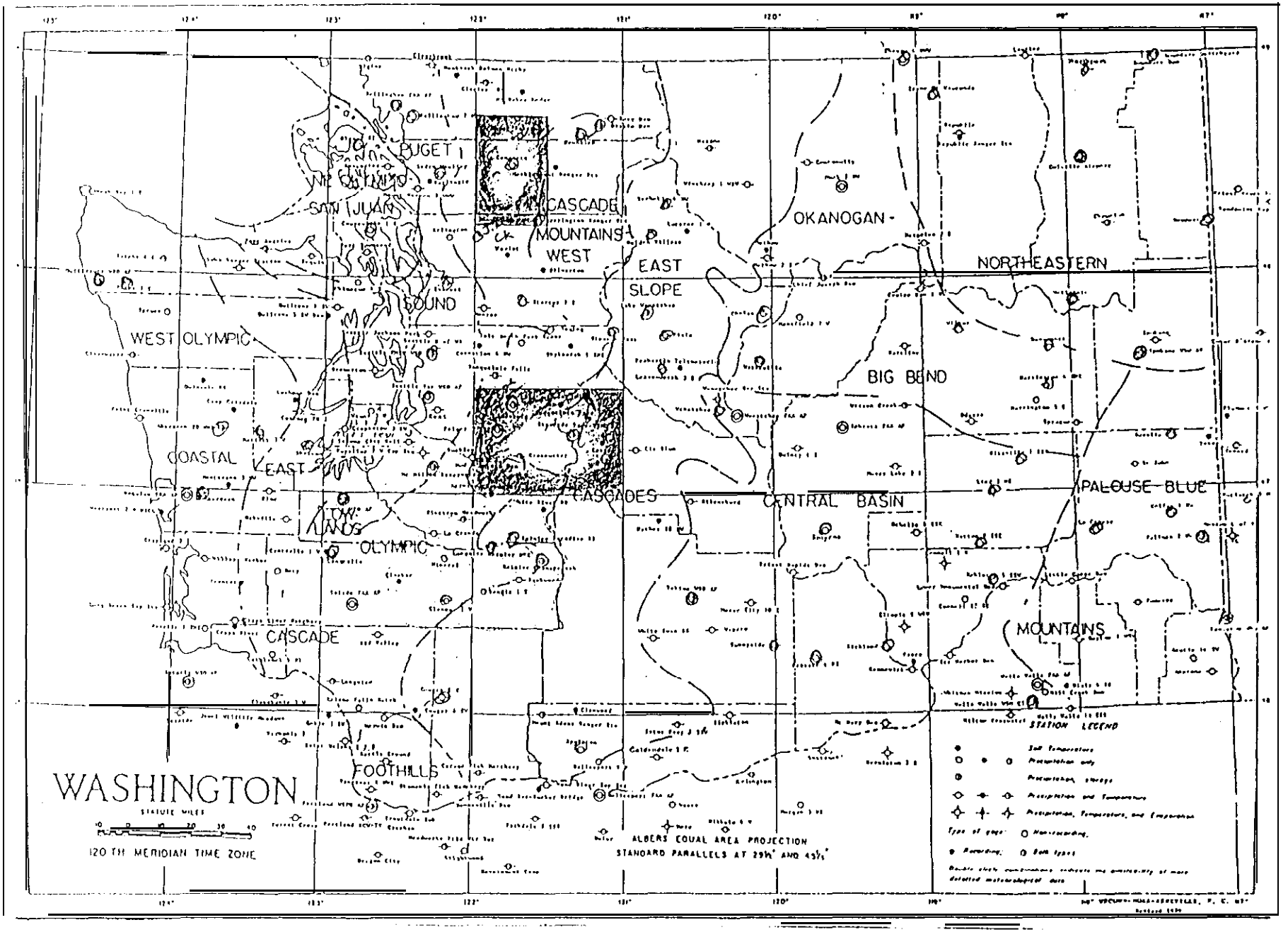

Fig. 1 Location of Mapped Areas

Figure 2a: Snowlines on Elevation Map

Snoqualmie Site, 16 Dec. 88

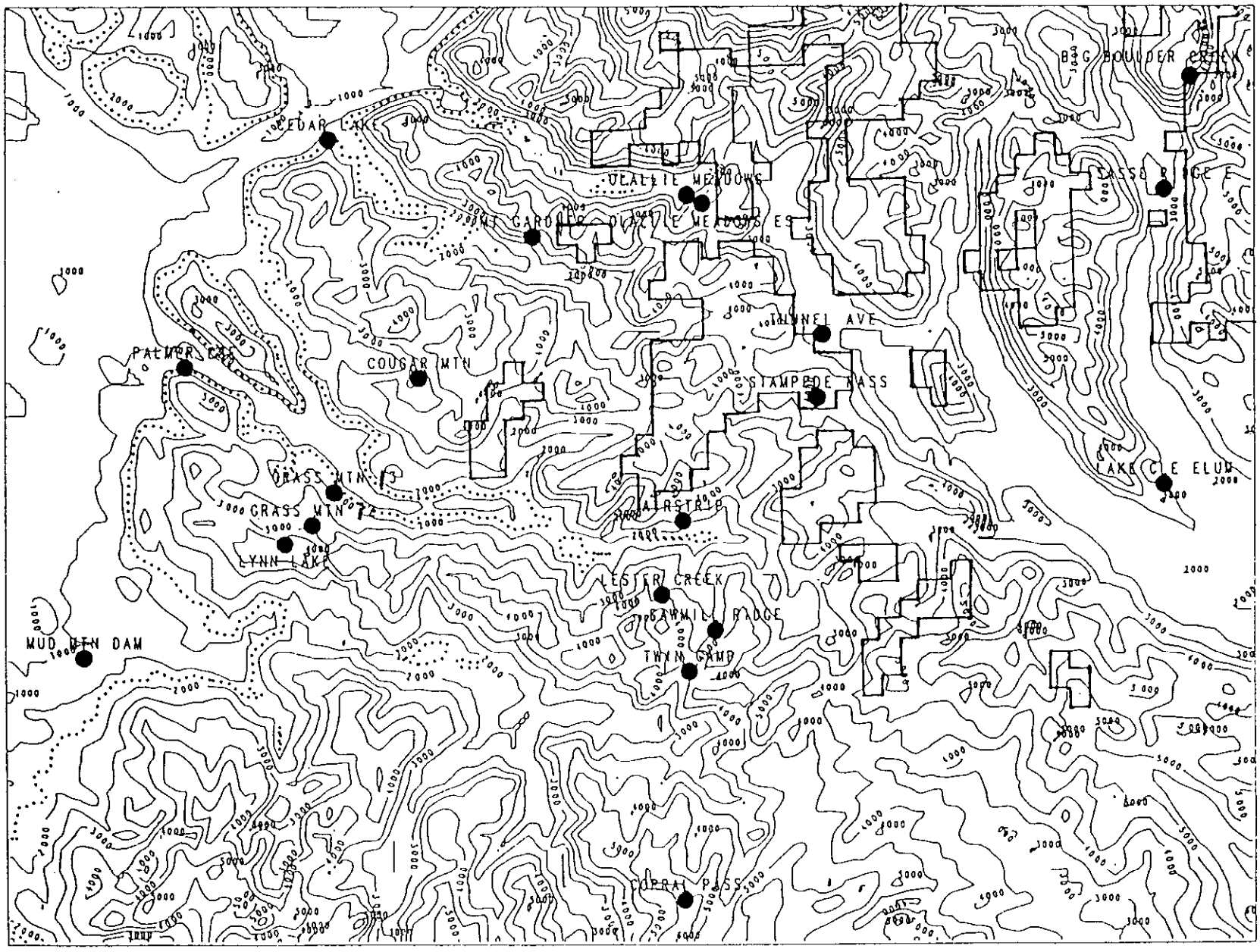

Figure 2b: Snowlines on Elevation Map
Snoqualmie Site, 8 Feb. 89

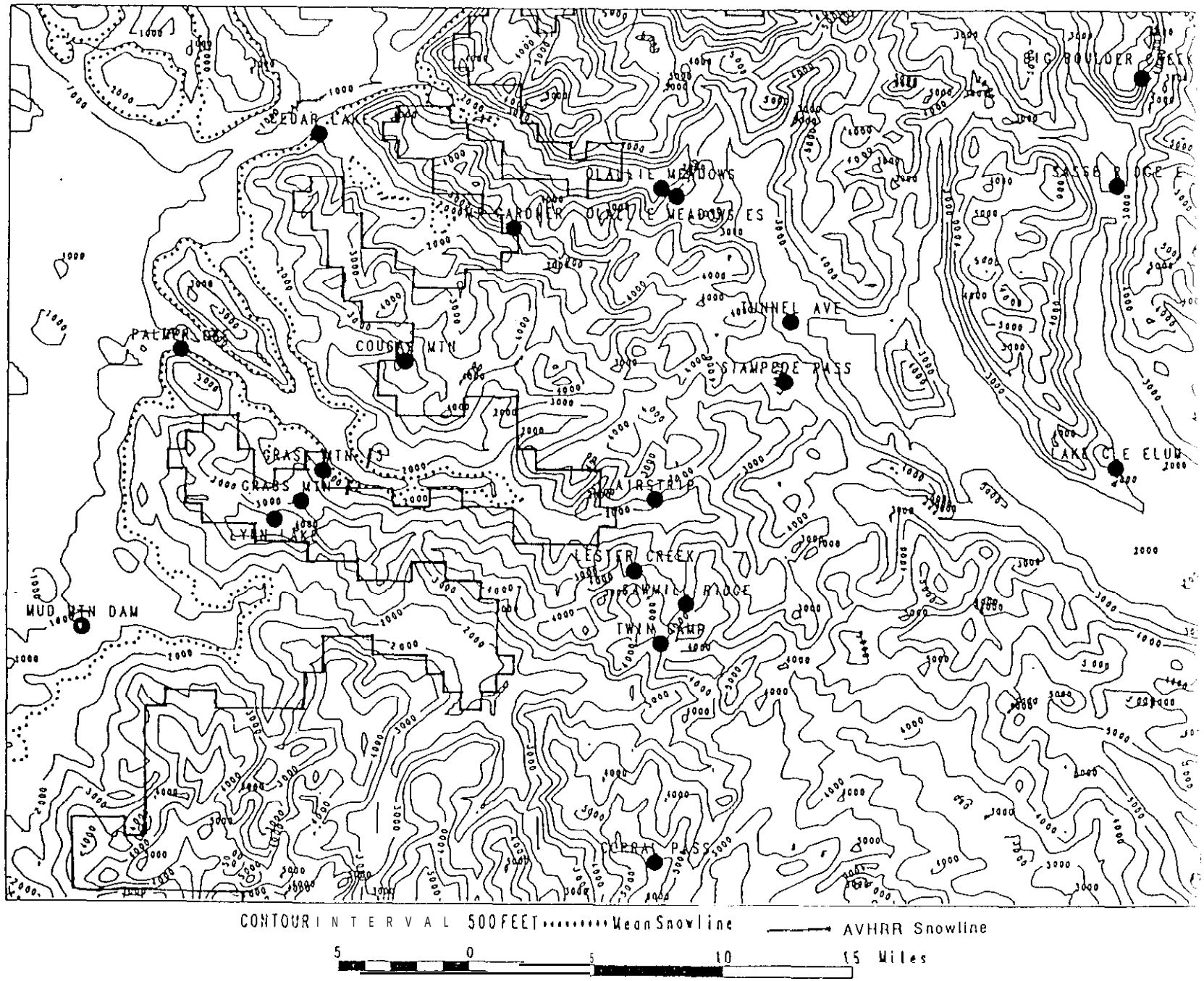

Figure 2c: Snowlines on Elevation Map
Concrete Site, 16 Dec. 88

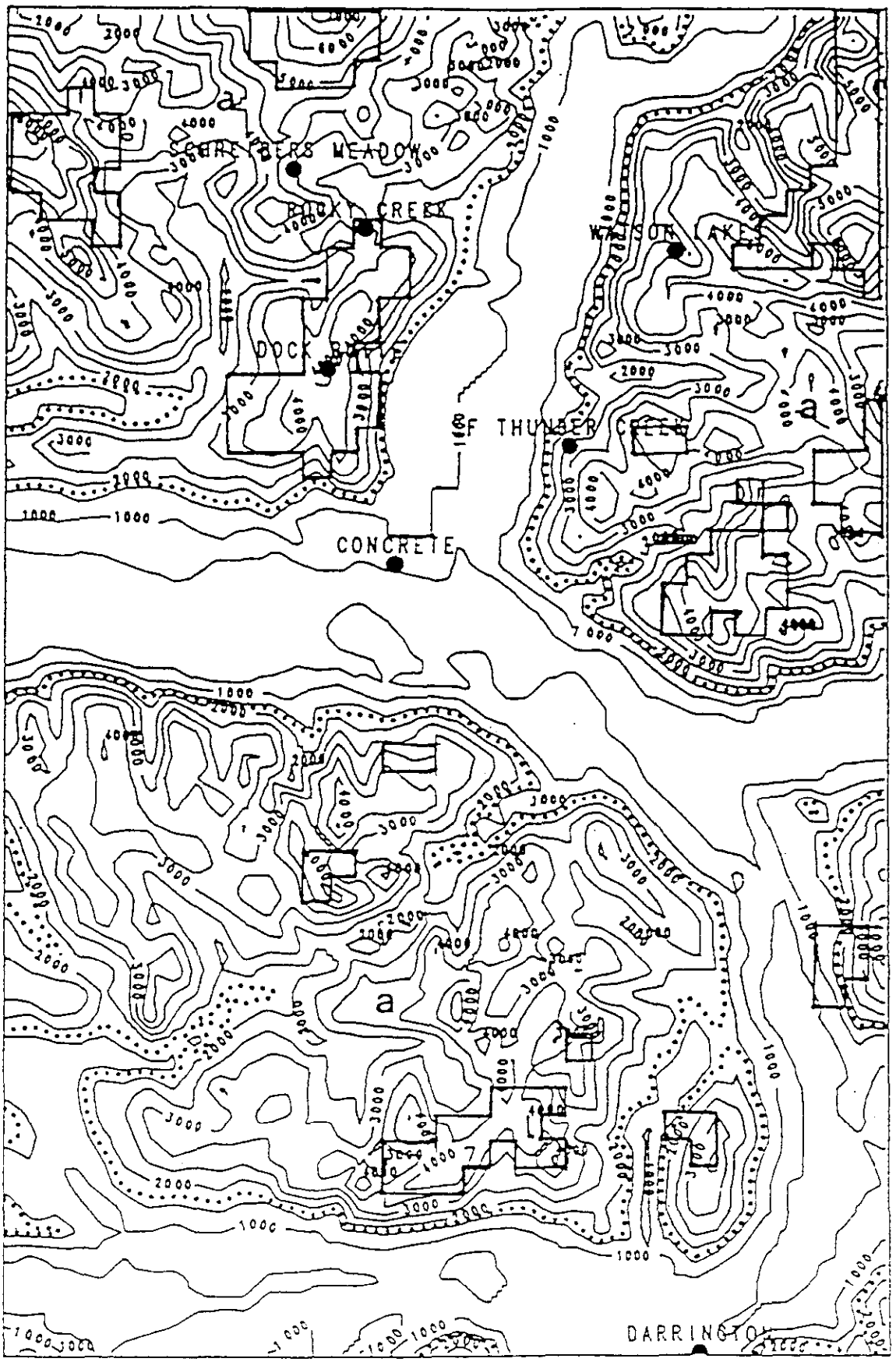

Figure 20: Snowlines on Elevation Map

Concrete Site, 8 Feb. 89

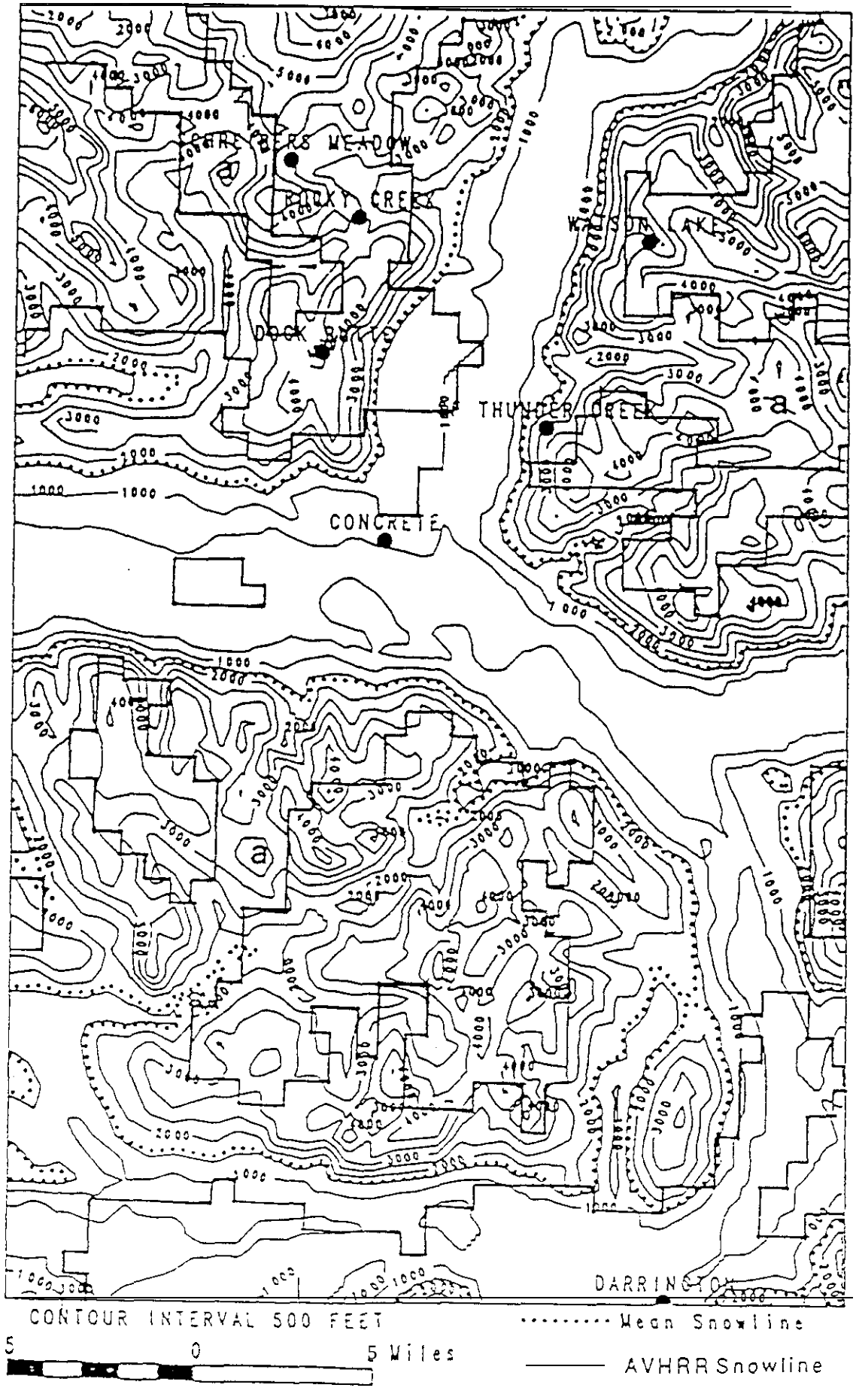

Figure 2e: Snowlines on Elevation Map

Concrete Site, 12 Apr 80

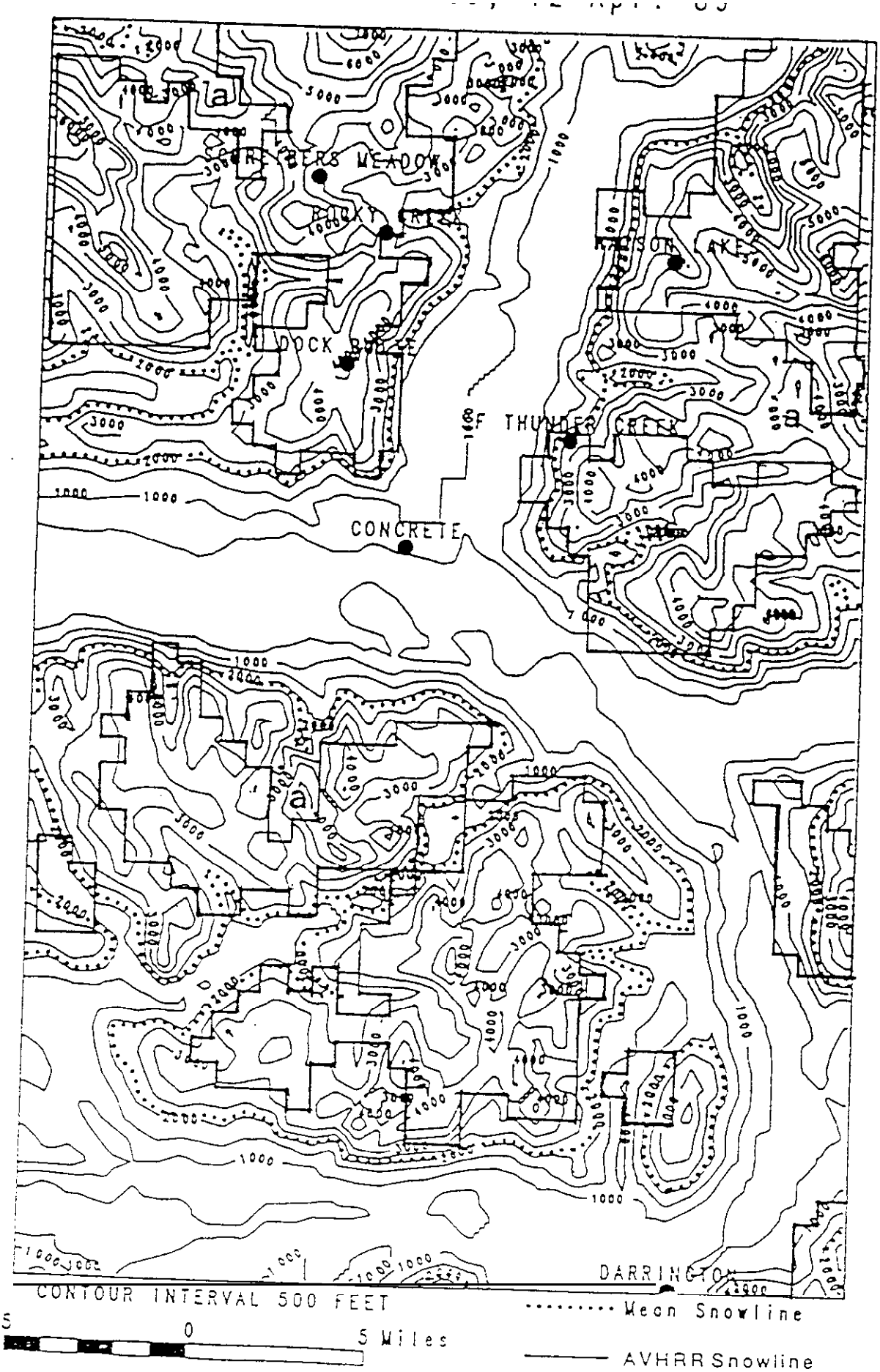

Figure 3a: Mean Snow Depth and Snowlines
Snoqualmie Site, 16 Dec. 88

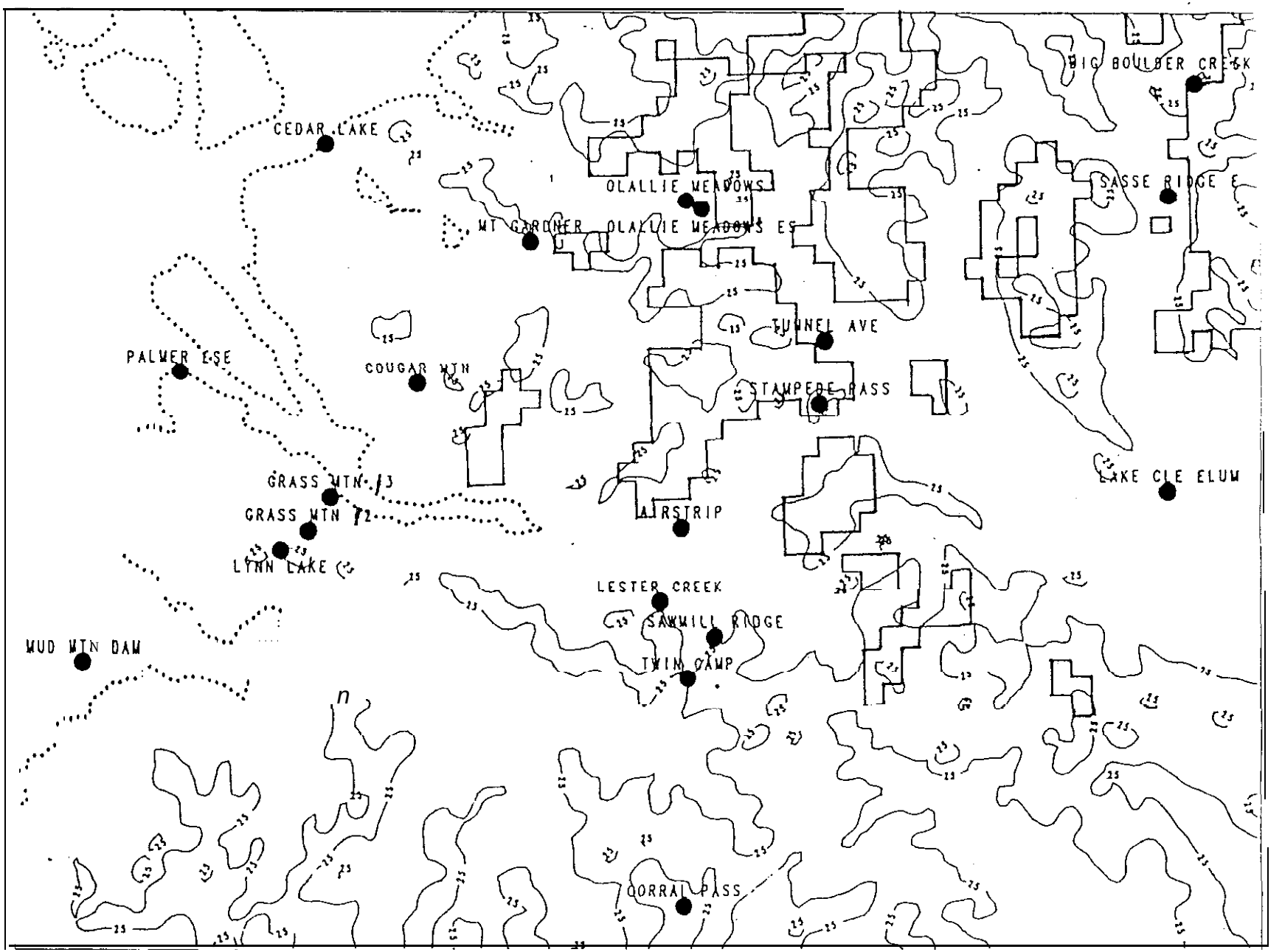

Figure 3b: Mean Snow Depth and Snowlines

Snoqualmie Site, 8 Feb. 89

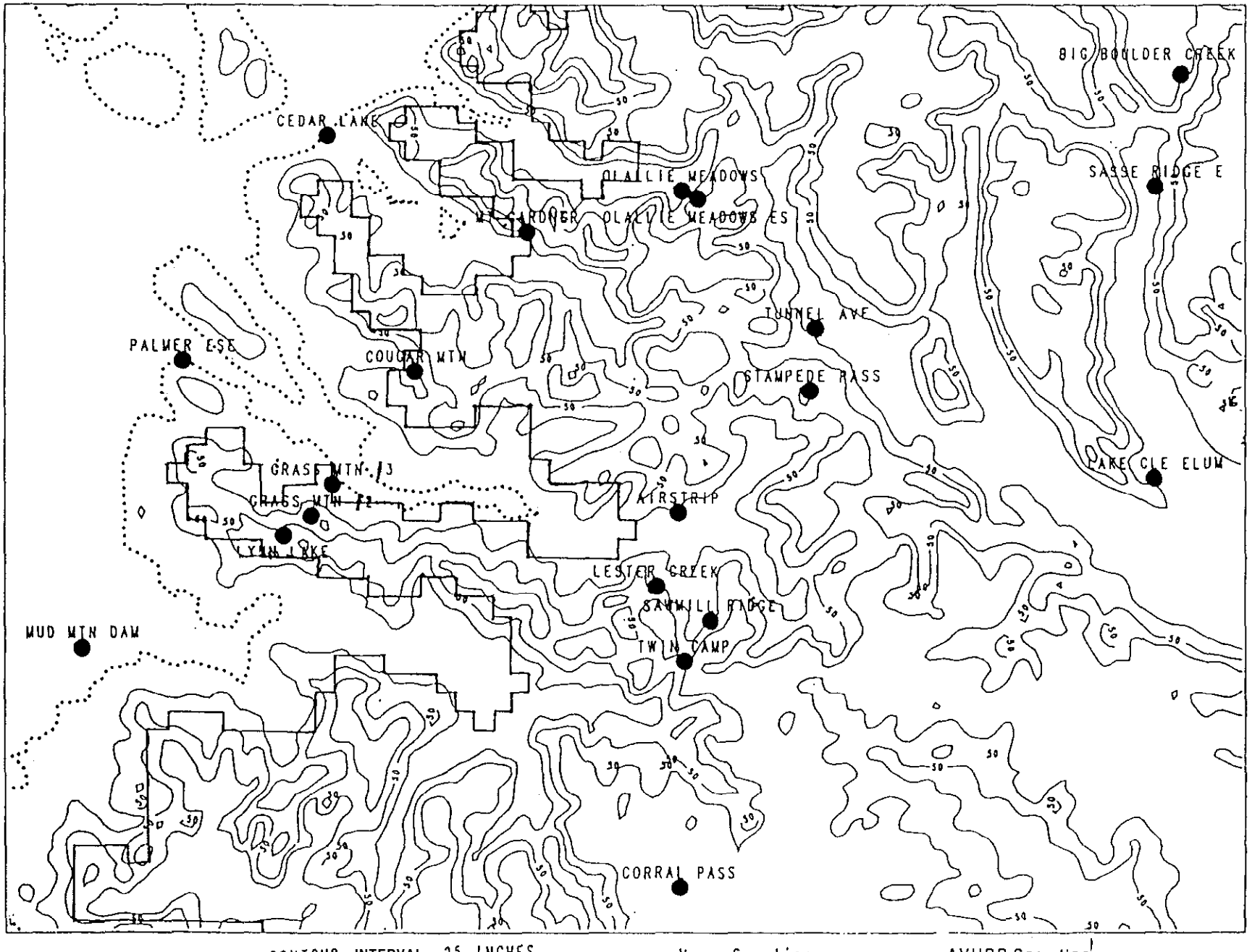

rigure 3c: Mean Snow Depth and Snowlines
Concrete Site, 1‘6 Dec. 88

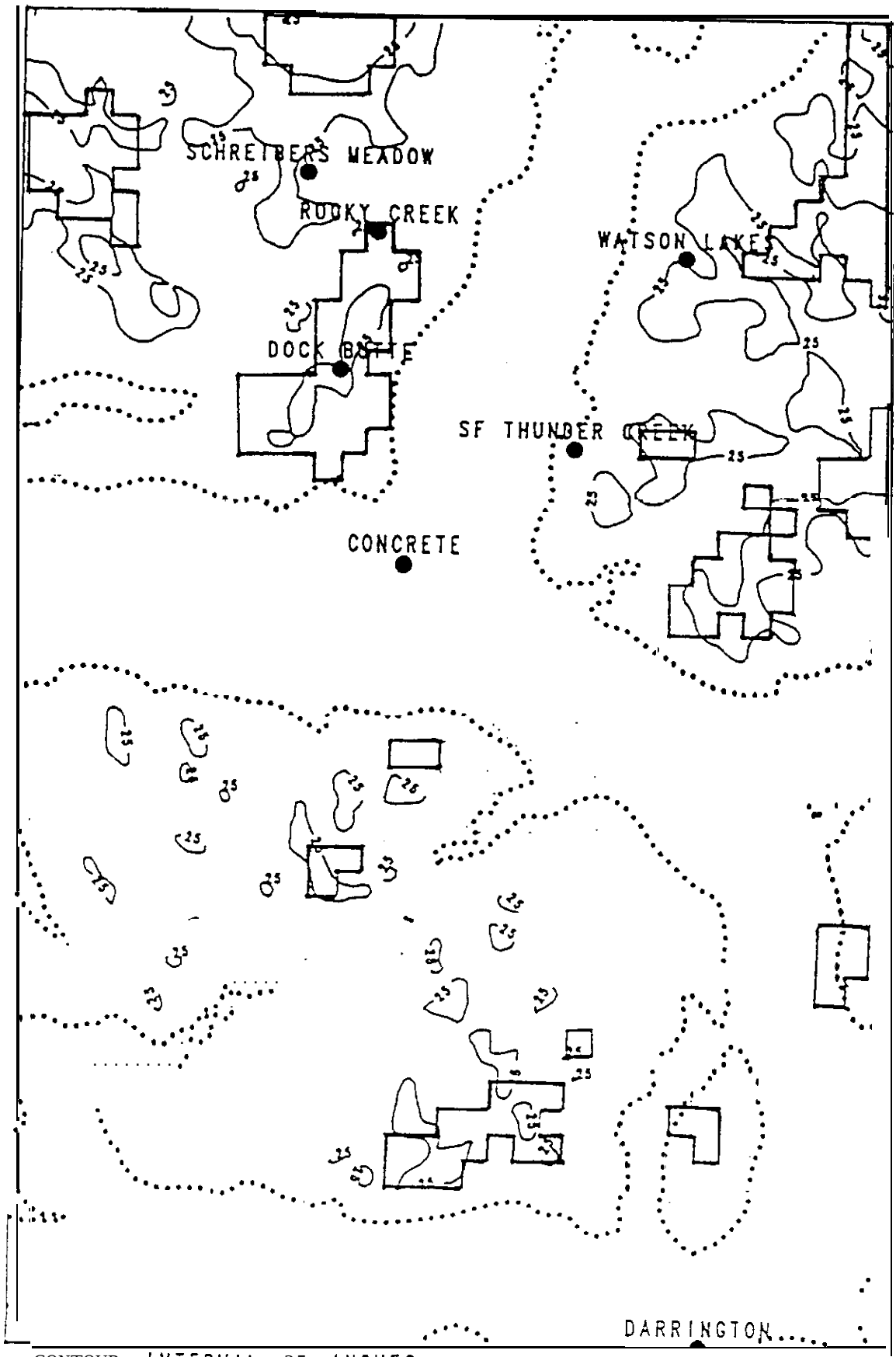

36

Figure 3a: Mean Snow Depth and Snowlines
Concrete Site, 8 Feb. 89

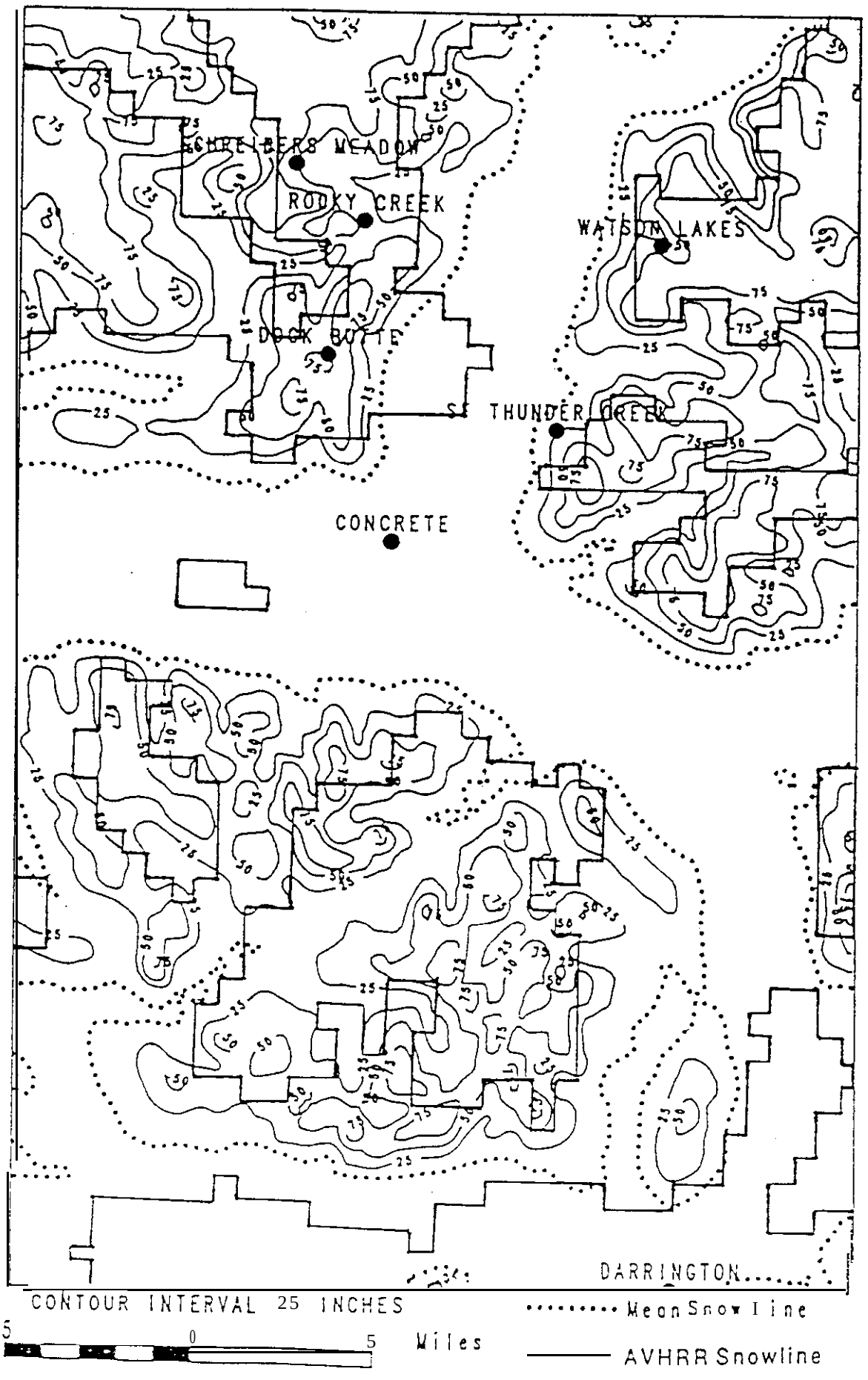

Snow Depth and Snowlines
Concrete Site, 12 Apr. 89

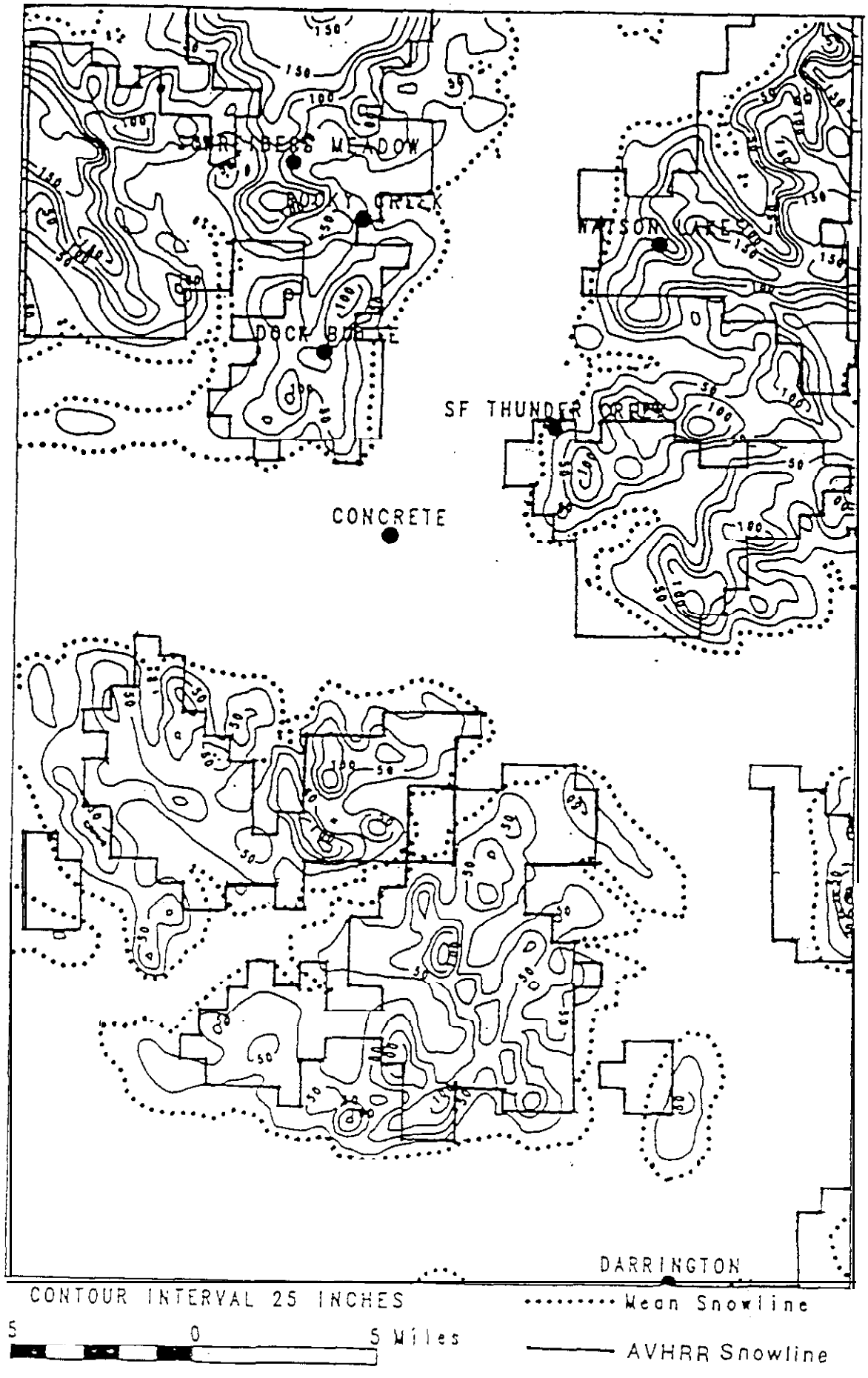

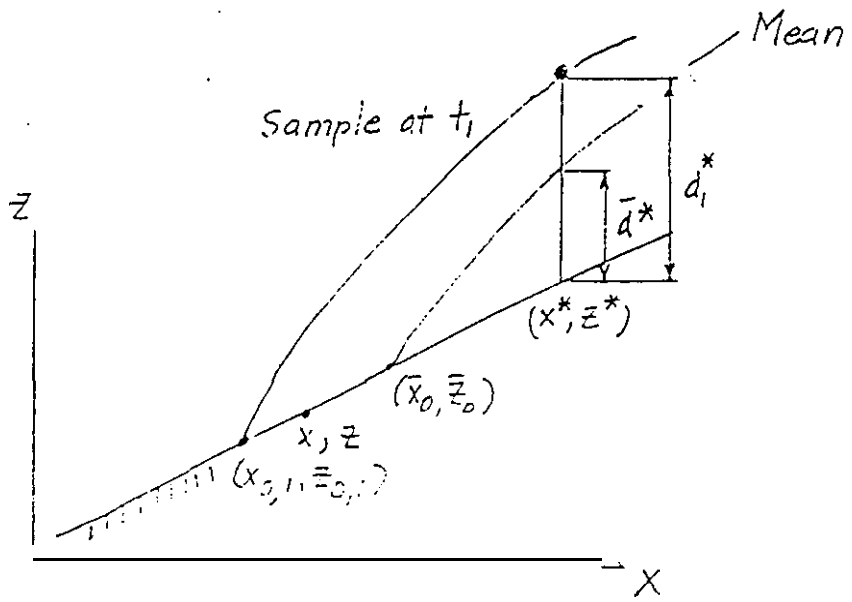

Fig. 4. Relationship between Snow Line and Snow Depth

Fig. 4

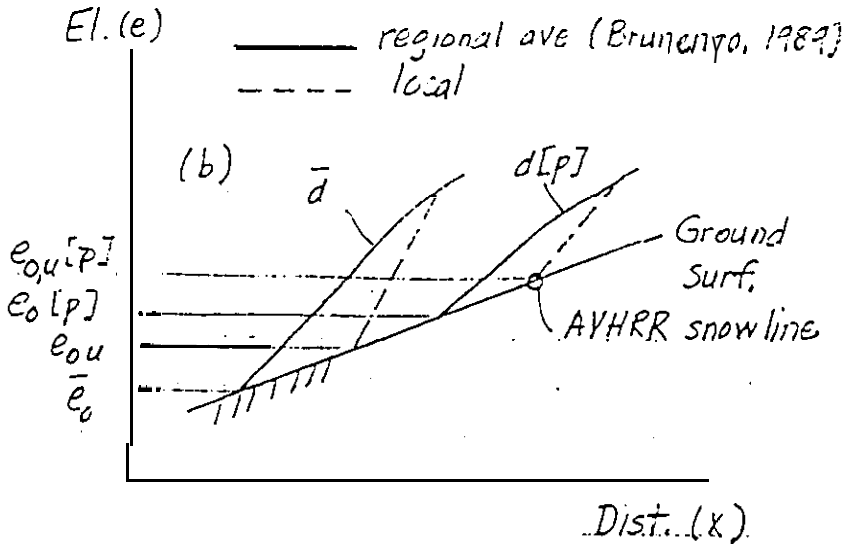

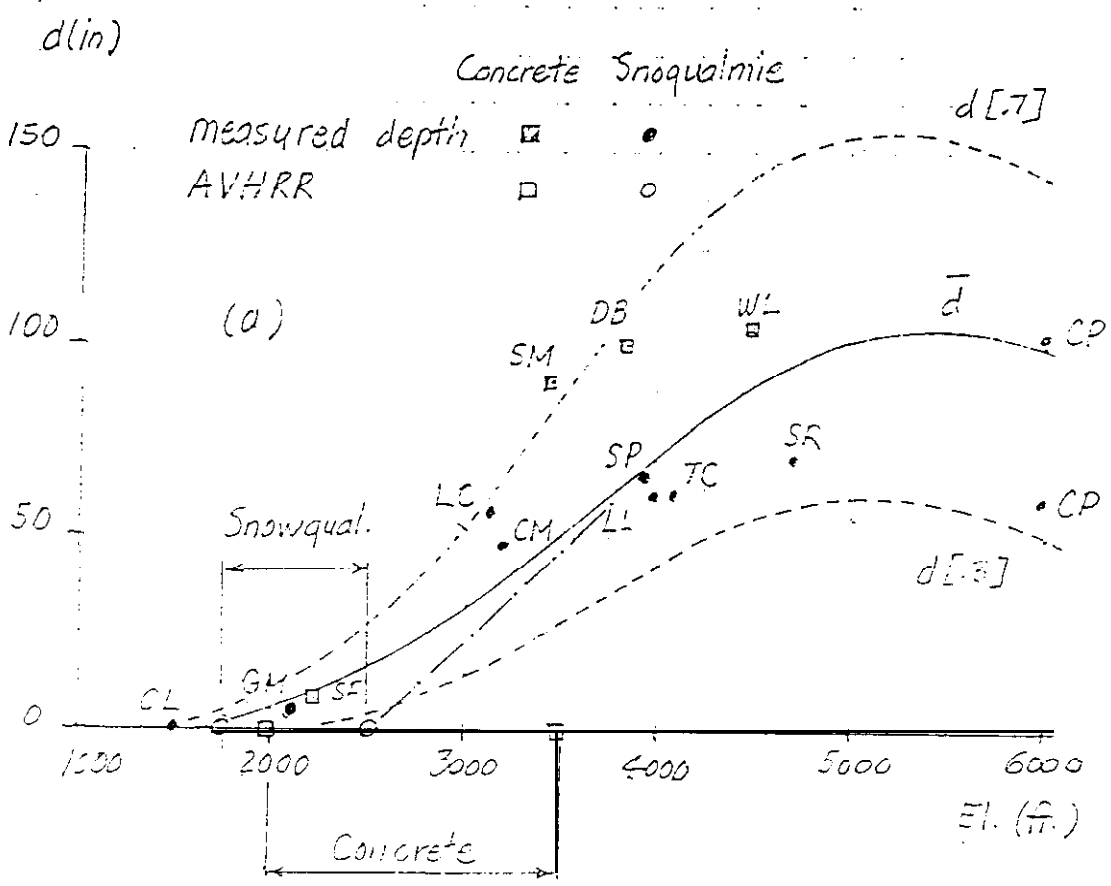

Figure 5. Snowline and Snow Depth versus Elevation (a) Measured and Computed Snow Depth and AVHRR Snowline. (b) Mean Snow Depth and Snow Depth with Probability p.

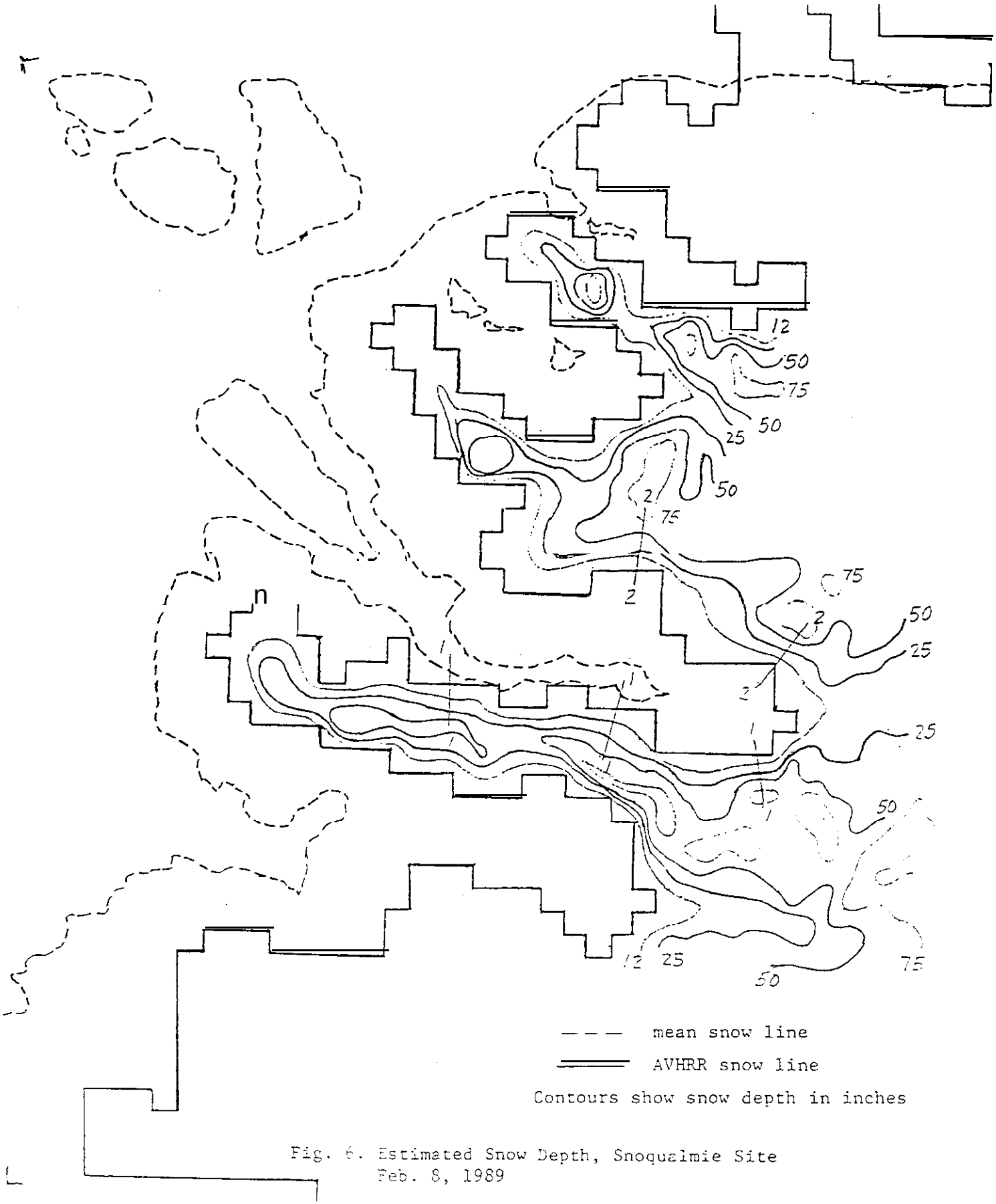

Fig. 6. Estimated Snow Depth, Snoqualmie Site
Feb. 8, 1989

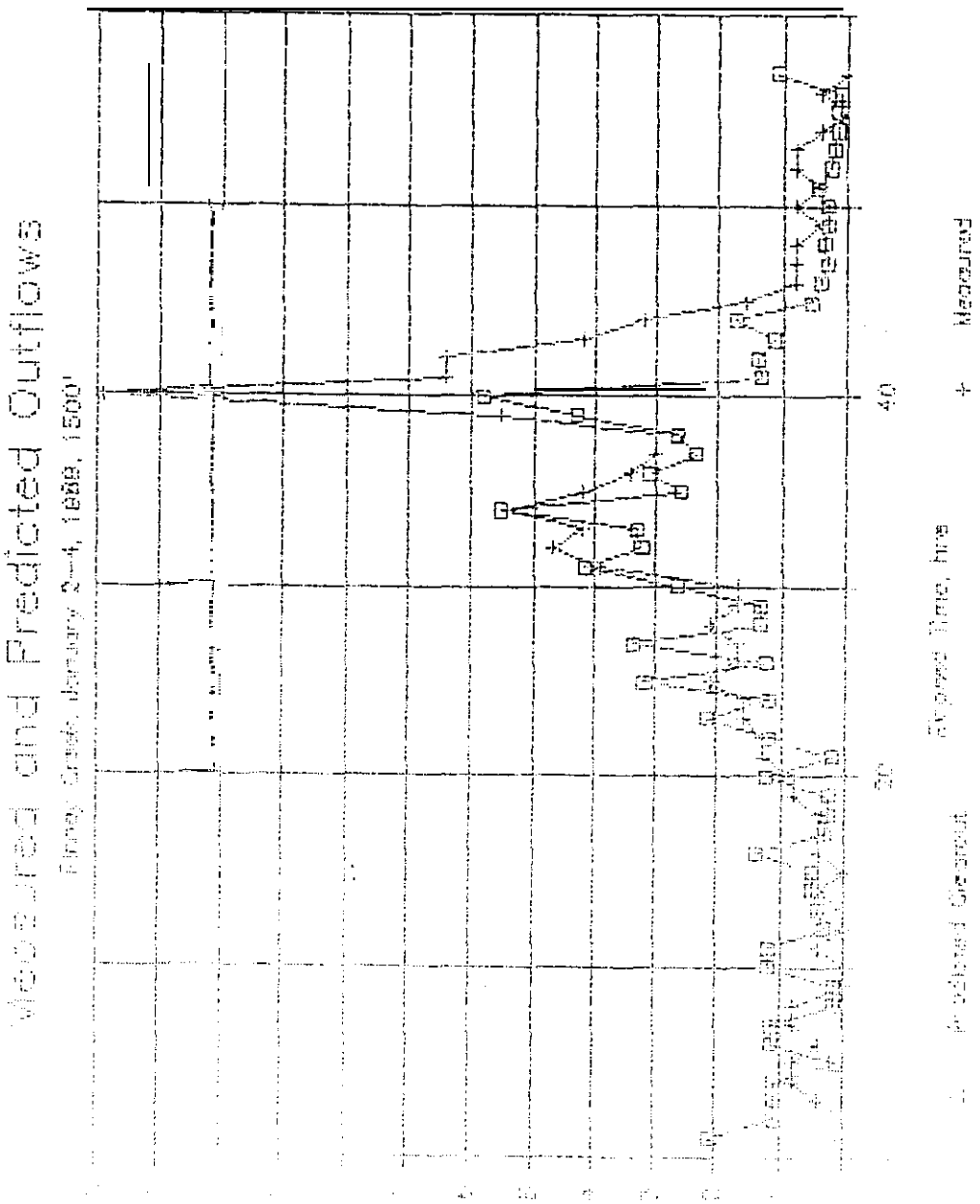

Fig.7. Computed and Measured Snomelt, Jan. 2-3-4,1989
Concrete Site.

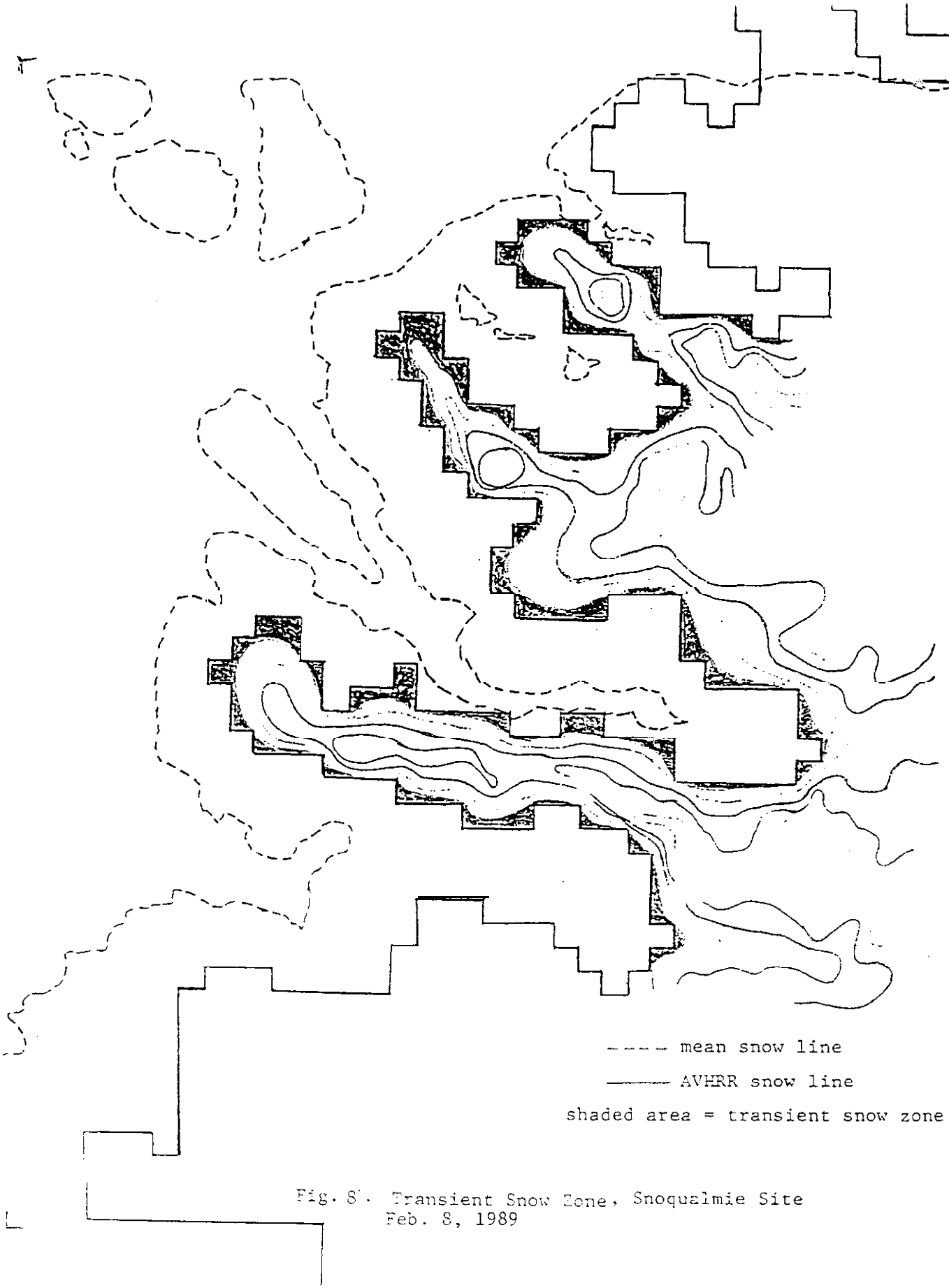

Fig. 8. Transient Snow Zone, Snoqualmie Site
Feb. 8, 1989

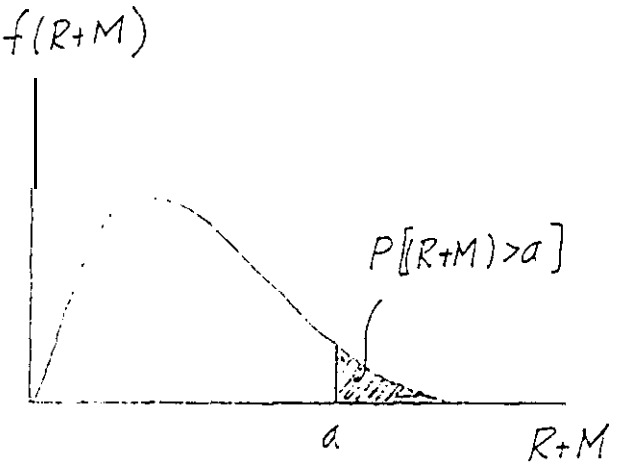

Figure 9. Probability Density Function for Rain Plus Snowmelt